Stochastic Spatio-Temporal Hurricane Impact Analysis for Power Grid Resilience Studies

John W. Muhs, Masood Parvania

Department of Electrical and Computer Engineering
University of Utah, Salt Lake City, UT 84112
Email: {john.muhs, masood.parvania}@utah.edu

Abstract—This paper develops a spatio-temporal hurricane impact analysis (STHIA) tool to assist power industry stakeholders in quantifying hurricane damage to the power grid. The STHIA model generates stochastic hurricane scenarios based on historical hurricane data, and maps likely outage scenarios to inland distribution components using component-specific structural information expressed by fragility curves. The outage scenarios generated by the STHIA model enable its user to identify potential risks to the power grid in the hours or days leading up to an impending hurricane event. Further, the STHIA model can be used as a contingency planning tool in order to identify grid-hardening measures.

Index Terms—Resilience, hurricane model, natural disaster, spatio-temporal modeling, power distribution system.

I. INTRODUCTION

Protecting coastal communities from hurricanes is becoming an increasingly costly endeavor for the United States [1]. Damages from three hurricanes in recent history, Katrina, Harvey, and Maria, incurred an estimated combined total cost of $341.6B [2]. Prolonged power outages resulting from high-impact low-probability events also pose a major concern to social welfare as the US population becomes increasingly urban and dependent on electric power. According to [3], nearly one-third of Puerto Rico's power customers were without power four months after Hurricane Maria made landfall. Customers in many rural areas were not expected to receive power until 8 months after Hurricane Maria occurred. As coastline demographics shift in the US, these high and increasing figures become easier to rationalize. Approximately 18.5% of the US population live in coastal counties along the US Atlantic seaboard, and the population in these counties is increasing by approximately 9.4% per decade [4]. Population growth as well as the high density of power infrastructure associated with urban areas in hurricane-prone regions presents a risk to power industry stakeholders, and consequently to the US economy. At the time of this paper's writing, hurricane Florence is making a devastating impact on the Carolina coast with power outages expected to affect millions of people [5].

To address the power industry stakeholders' needs, understanding, quantifying and exploring ways to enhance the resilience of power systems against natural disasters (e.g., hurricane) has became a focus for many researchers, practitioners and policy makers in academia, industry and governments [6], [7]. In recent years, multiple power grid resilience studies have been conducted to mitigate impacts of severe weather events, which include efforts for conceptualizing metrics, infrastructure and resource planning, use of distributed energy resources, and resilient microgrid operations [8]–[14]. Preventative grid hardening measures such as structural reinforcement and line undergrounding are often implemented to mitigate impact from hurricanes, but these methods can be costly at a large scale, and should be economically justified [15]. Consequently, disaster simulations and impact modeling are necessary to foster prudent decision-making by power industry planners when considering resilience-enhancing options.

Sufficient historical data exists, through databases such as the NOAA HURDAT database [16] to quantify historical hurricane behavior, and to use this information to forecast hurricane-related risks in the future. To date, however, publicly-available models to quantify the impacts of hurricanes on power systems are limited. HAZUS, a tool developed by the U.S. Federal Emergency Management Agency (FEMA), is the most widely-used publicly available hurricane simulation software, however its simulations focus on quantifying costs resulting from damage to the built-environment, not damage to power infrastructure [17].

This paper presents a model for stochastic spatio-temporal hurricane impact analysis (STHIA) that generates and analyzes a large number of random hurricane events to be used in two prevalent power grid resilience studies. First, the STHIA model could forecast potential scenarios in the hours or days leading up to an impending hurricane event. In this case, hurricane path and strength are assumed to have been forecasted to some degree of certainty, which can be used as inputs to the model. Second, the STHIA model can be used as a general contingency planning tool in order to identify grid-hardening measures. For the latter, historical hurricane data can be used to simulate possible hurricane scenarios for the long-term future.

The remainder of this paper is presented as follows. Section II presents an overview of structure and modules of the proposed STHIA model. Section III presents the formulation of the spatio-temporal hurricane simulation model. Section IV presents the implementation of fragility curves and component locations to create a spatio-temporal grid impact model. Numerical results of a case study with 1000 randomly generated scenarios are presented in Section V. Section VI concludes the paper and discusses the future work.

II. STHIA: STOCHASTIC SPATIO-TEMPORAL HURRICANE IMPACT ANALYSIS

This section presents the proposed model for stochastic spatio-temporal hurricane impact analysis (STHIA) for power grid resilience studies. The proposed model is composed of two major sequential modules: 1) spatio-temporal hurricane simulation, 2) grid component impact analysis. The proposed model calculates stochastic grid component outage scenarios as a result. The components of the proposed model with the associated inputs are shown in Fig. 1, and are described next.
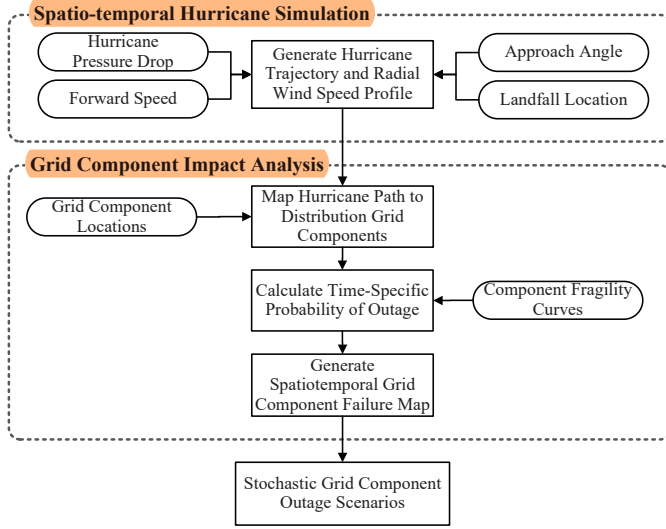

Fig. 1. Stochastic spatio-temporal hurricane impact analysis (STHIA) model

1) Spatio-Temporal Hurricane Simulation: This module integrates a mathematical hurricane model in order to simulate spatio-temporal hurricane path and strength using historical data. Two primary hurricane characteristics, namely hurricane strength (i.e., wind speed) and temporal path, are most important when modeling the impact on the distribution grid. The hurricane characteristics are defined as a set of statistical curve shape parameters as will be further discussed in Section III and implemented in Section V.

2) Grid Component Impact Analysis: The grid component impact analysis module in Fig. 1 utilizes the locations and structural properties of the grid components for quantifying the impacts of a hurricane on a proximate power distribution grid. A vector between location of the grid component, and the changing location of the hurricane eye is used to determine the component-to-eye distance. This distance is then mapped to the radial wind speed curve in [18] to calculate the wind speed experienced by each component over the time horizon being considered. The structural property of a distribution component, expressed as a fragility curve, is then utilized to calculate its failure probability as a function of wind speed [8], [19].

3) Calculating Stochastic Grid Component Outage Scenarios: Using a spatio-temporal hurricane simulation and component-specific fragility curves, the STHIA model cal-

culates spatio-temporal component failure probabilities. The closer the component is to the hurricane eye wall (where max wind speeds occur), the higher the component's probability of failure. A Monte Carlo method is then utilized to generate temporal component failure scenarios. With large numbers of scenarios generated through the Monte Carlo method, the aggregate scenarios are weighted towards the probabilistic inputs of the model, allowing the user to understand likely component outage scenarios and their associated probability.

III. SPATIO-TEMPORAL HURRICANE SIMULATION

This section presents the details of the spatio-temporal hurricane simulation module in Fig. 1. The hurricane simulation model includes a hurricane radial wind profile scenario that is mapped to a scenario-specific temporal hurricane path. Then, a vector spanning from the center of the hurricane (the *eye*) to any location on the map denotes that location's radius to the eye of the hurricane. The resulting radial distance is then used to determine the wind speed at a given location. The formulation utilized to generate the wind speed profile and the temporal hurricane path scenarios is presented next.

A. Hurricane Wind Speed Profile

Hurricane eye pressure difference is a metric determined by atmospheric scientists to understand the characteristics relating to hurricane size and strength. The probability of hurricane eye pressure difference is mathematically defined by the Weibull distribution [20], [21]:

$$p(\Delta P_s) = \frac{k}{C}\left(\frac{\Delta P_s}{C}\right)^{k-1} e^{-(\Delta P_s/C)^k}, \quad (1)$$

where ΔP_s is the hurricane eye pressure difference, subscript s is the index of scenarios, k is the Weibull shape parameter and C is the Weibull scale parameter. The hurricane eye pressure, P_s^{eye}, can then be defined as the difference between the average sea level pressure, P^{atm}, and the hurricane eye pressure difference from (1):

$$P_s^{eye} = P^{atm} - \Delta P_s \quad (2)$$

where P^{atm} is approximated as 1013 mbar. Using this hurricane central pressure, the corresponding maximum sustained wind speed, $\overline{V_s}$, is determined by interpolating in the Saffir-Simpson table [22] given in Table I.

TABLE I
SAFFIR-SIMPSON TABLE

Hurricane Category	Central Pressure [mbar]	Wind Speed [m/s]
1	>979	33-42
2	965-979	43-49
3	945-964	50-58
4	920-944	58-70
5	<920	>70

A theoretical hurricane wind profile, presented in [18], [23], takes the maximum sustained wind speed, $\overline{V_s}$, as an input and

defines wind speed of a hurricane as a function of distance from its eye, which is formulated in (3)-(7):

$$V_s(r) = \left[\frac{AB(\Delta P_s)e^{-A/r^B}}{\rho r^B} + \frac{r^2 f^2}{4}\right]^{1/2} - \frac{rf}{2} \quad (3)$$

$$A_s = R_s^{max\,B_s} \quad (4)$$

$$B_s = \frac{\overline{V_s}^2 \rho e}{\Delta P_s} \quad (5)$$

$$R_s^{max} = e^{2.556 - 0.000050255\Delta P_s^2 + 0.042243032\phi} \quad (6)$$

$$f = 2\Omega\phi \quad (7)$$

where A and B are shape parameters of the profile expressed in (3), r is the radius from hurricane center, ρ is density of air, R_s^{max} is radius to max wind, Ω is the Earth's angular velocity, and ϕ is the storm latitude.

B. Temporal Hurricane Path

The temporal hurricane path is defined by three characteristics: 1) approach angle, 2) landfall location, and 3) translation velocity. The approach angle and landfall location determine the temporal hurricane path that is assumed to be linear. The hurricane's translation velocity, which is defined as the translation movement speed of the hurricane eye, gives the hurricane path its temporal dimension. Therefore, generation of the temporal hurricane path allows the location of the hurricane to be determined for every time step in the simulation. Similar to hurricane eye pressure difference, this value will be stochastically for each hurricane scenario. In order to model this uncertainty, a random value is selected for each of the temporal hurricane characteristics based on their respective associated probability distribution functions [20], [21], [23]:

$$p(\Phi_s) = \frac{1}{\sqrt{2\pi}\sigma_\phi}e^{-\frac{1}{2}[(\phi_s - m_\phi)/\sigma_\phi]^2} \quad (8)$$

$$p(\Delta x_s) = \frac{1}{\sqrt{2\pi}\sigma_x}e^{-\frac{1}{2}[(\Delta x_s - m_x)/\sigma_x)^2]} \quad (9)$$

$$p(c_s) = \frac{1}{c_s\sqrt{2\pi}\sigma_{lnc}}e^{-\frac{1}{2}(ln(c_s) - m_{ln})/\sigma_{ln}} \quad (10)$$

where hurricane approach angle, Φ_s, and landfall location, Δx_s, are expressed by normal probability distribution functions (PDFs) in (8) and (9), and translation velocity, c_s, is expressed with a lognormal PDF in (10). For each of these parameters, mean m and standard deviation σ are calculated based on historical data. The translation velocity, approach angle, and landfall location are mapped to every time period, t, in the time horizon, NT, to calculate the temporal location of the hurricane in (11), (12):

$$Y_{s,t} = c_s t - \frac{Y_s^{tot}}{2} \quad (11)$$

$$Y_s^{tot} = c_s NT \quad (12)$$

where $Y_{s,t}$ is the temporal location of hurricane at time t, Y_{tot} is the total distance traveled by the hurricane in the horizon. The initial location of the hurricane is set to half of its total distance traveled such that the hurricane makes landfall approximately half way through the horizon.

IV. GRID COMPONENT IMPACT ANALYSIS

The grid component impact analysis module in Fig. 1 includes three steps:1) determining the distance of each grid component to the hurricane eye, 2) generating a wind speed curve at each component location, and 3) correlating wind speed values to component-specific fragility curves to determine the probability of failure for each grid component. The steps are discussed in detail next.

A. Spatio-temporal Component Distance to Hurricane Eye

In order to map the wind speed to each grid component, we need to define the spatio-temporal distance between the component and the hurricane. This spatio-temporal distance can be expressed as the component-to-eye vector. We assume that all grid components are mapped on a 2-dimensional plane and neglect the curvature of the Earth, although earth's curvature could be implemented in future works. The expected landfall location is defined as the origin of the coordinate system. For simplicity, we do not reference the cardinal directions (North, South, etc.), but consider a Cartesian plane aligned on an assumed straight coastline as shown in Fig. 2.
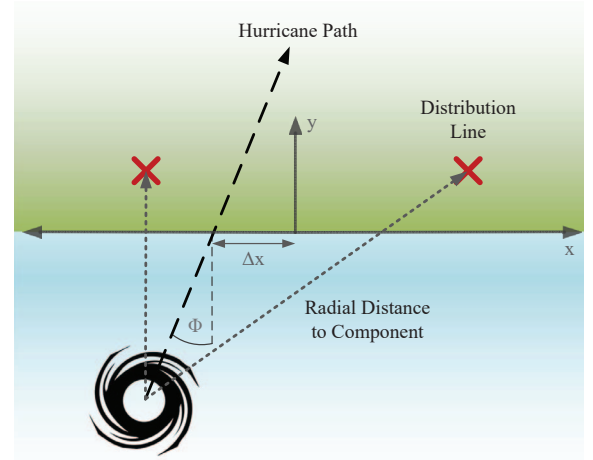

Fig. 2. Cartesian coordinate system and vectors used to determine locations of the grid components relative to hurricane eye

All component locations are initially specified in terms of their proximity to the expected landfall location as x_i and y_i where i is the index of grid component. However, by shifting the coordinate system by the approach angle Φ, the locations of grid components can be expressed in terms of rotated vectors, $x'_{i,s}$ and $y'_{i,s}$, with are aligned with the hurricane path. By use of Pythagorean Theorem on $x'_{i,s}$ and $y'_{i,s}$, the magnitude of the component-to-eye vector, $D_{i,t,s}$, between the hurricane eye and the component can be calculated as demonstrated in (15):

$$x'_{i,s} = (x_i + \Delta x_s)\cos(\phi_s) + y_i\sin(\phi_s) \quad (13)$$

$$y'_{i,s} = -(x_i + \Delta x_s)\sin(\phi_s) + y_i\cos(\phi_s) \quad (14)$$

$$D_{i,t,s} = \sqrt{(Y_{s,t} + y'_{i,s})^2 + (x'_{i,s})^2} \quad (15)$$

B. Component Wind Speed Curve

Before landfall, the hurricane is assumed to have a constant central pressure and thus constant radial wind profile. While the hurricane remains over water, a time-based wind speed curve can simply be generated by plugging in the hurricane-to-component vector $D_{i,t,s}$ into the radial wind speed profile formula in (3). However, after the landfall has occurred, the strength of the hurricane decays based on the wind-speed decay function in (16):

$$V_{i,t,s} = V^b + (V_s(D_{i,t,s})R - V^b)e^{-\alpha(t-T_s^0)} \qquad (16)$$

where V^b denotes a background sustained wind speed in the hours following a hurricane event set to 13.735 m/s, α is the decay constant set to 0.095 per hour, R is a wind speed reduction factor set to 0.9, and T_s^0 denotes the time period in which the hurricane makes landfall. The values of parameters V^b, α, R and vary by region [24]. This paper assumes that the hurricane decays equally at all values of hurricane radius. Considering wind speed decay is vital to avoid overestimating wind speeds for grid components further inland.

C. Mapping to Component Fragility Curve

Component-specific fragility curves can be used in conjunction with the component wind speed curve to quantify the temporal failure probability of each grid component. Fragility curves are commonly represented by a normal or lognormal CDF. Finite element analysis is typically used to generate line fragility curves. Historical failure data is also used in [19] to generate similar curves to represent structural failure properties of wooden utility poles. As specific fragility curve parameters were unavailable to the authors, the fragility curves used in this paper were repesented by a linear approximations of CDFs as shown in Fig 3.
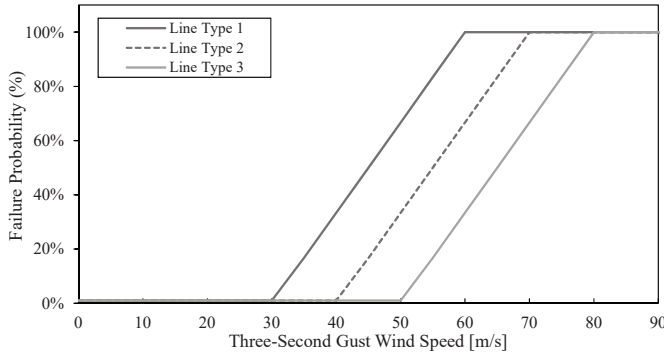

Fig. 3. Fragility curves representing three types of distribution lines

For each time period, the wind speed value from the component wind speed curve is mapped to the component's fragility curve. The failure probability is calculated as:

$$p_{i,t,s}^{fail} = \begin{cases} 1 & \text{if } V_{i,t,s}^{gust} \geq v_i^{up} \\ 0 & \text{if } V_{i,t,s}^{gust} \leq v_i^{lo} \\ p(v_{i,t,s}) & \text{if } v_i^{lo} < V_{i,t,s}^{gust} < v_i^{up} \end{cases} \qquad (17)$$

where v_i^{lo} and v_i^{up} are the lower and upper bounds of fragility curves for each line type as in Fig. 3, and $V_{i,t,s}^{gust}$ is three-second gust wind speed that is calculated as $V_{i,t,s}^{gust} = 1.287 V_{i,t,s}$ [23]. Component failure scenarios are then determined by generating a uniformly distributed random variable $n_{i,s} \sim U(0,1)$. Line failure occurs if $n_{i,s} < p_{i,t,s}^{fail}$. Once a line fails, it remains failed for the remainder of the horizon.

V. CASE STUDY

In this study, 1000 hurricane scenarios are simulated in the Gulf-Coast region. The longitude and latitude of Houston, Texas (29.7604 N, 95.3698 W) were initialized as the expected landfall location. A 24-hour time horizon is considered at 5-minute intervals. Table II shows all inputs used in the hurricane model [23], and the locations and types of 10 hypothetical lines used in this study are given in Table III. The data in the Tables II and III were used as inputs to the STHIA model.

TABLE II
HURRICANE CHARACTERISTIC INPUTS

Hurricane Characteristic	Parameter	Value
Central Pressure Difference	C	33
	k	1.4
Approach Angle	m	0
	σ	10
Landfall Position	m	0
	σ	5
Translation Velocity	m	3.1
	σ	0.35

TABLE III
LINE TYPES IN CASE STUDY

Line ID	x [km]	y [km]	Line Type
1	60	50	1
2	55	50	1
3	50	50	1
4	-50	50	1
5	-55	50	1
6	30	20	2
7	25	20	2
8	20	20	2
9	20	10	3
10	20	15	3

For each scenario, a hurricane is simulated based on probabilistic inputs in Table II. Component wind speed curves were calculated using the component-to-eye vector and the hurricane wind speed profile. In Fig. 4, the wind speed increases as the eye of the hurricane approaches the component. The maximum wind speed is achieved when the distance between the component and the hurricane eye wall, denoted by R_s^{max} in (6), is minimized. Moreover, if the eye of the hurricane passes directly over the component location, as seen in Lines 6 and 9 in Fig. 4, the wind speed will be less than at the hurricane eye wall. Wind speed decay is visible in Fig. 4, which has a significant effect in reducing failure rates of inland components.
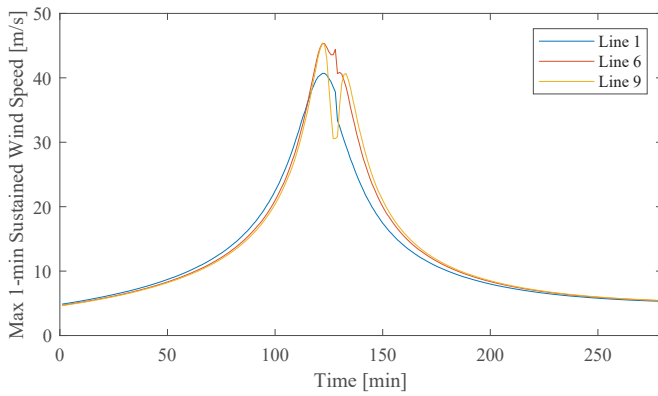
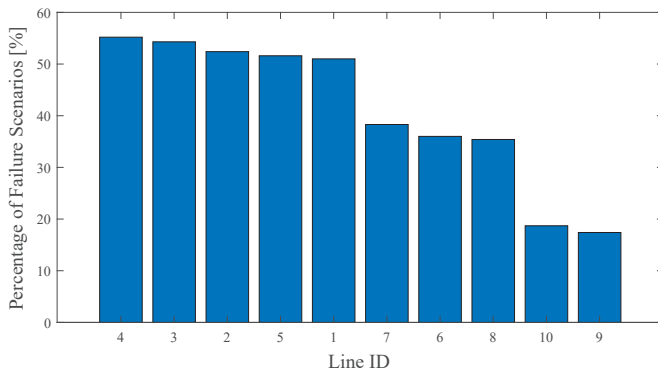Fig. 4. Wind speed curves compared for Lines 1, 6 and 9 in a single scenario

Fig. 5. Line outage occurrences from 1000 scenarios

In Fig. 5, the failure maps from the STHIA model are aggregated to show the percentage of scenarios in which lines experience failure. The lines are sorted with respect to failure occurrence, allowing the user to identify which lines have the highest failure probabilities. Two noteworthy factors seem to dictate line failure probabilities in the results: 1) the line's proximity to the hurricane path, and 2) the structural properties of the component expressed by its fragility curve. Lines closest to the expected landfall location fail more often than those farther away with equal structural properties.

VI. CONCLUSION

A stochastic spatio-temporal hurricane impact analysis (STHIA) model is proposed for failure analysis in the power distribution grid. A Monte Carlo simulation of 1000 hurricane scenarios is conducted to characterize distribution component failures and their associated probabilities for 10 hypothetical lines located in Gulf Coast region. The simulation results indicated that the lines closer to the expected hurricane path are at greater risk of failure. Thus, the application of the STHIA model supports component prioritization when considering available resilience-enhancing measures. Future works include improving the hurricane simulation by modeling a non-linear hurricane path and considering component restoration times.

REFERENCES

[1] R. J. Campbell, "Weather-related power outages and electric system resiliency." Congressional Research Service, Library of Congress Washington, DC, 2012.
[2] "Costliest u.s. tropical cyclones tables ubdated," NOAA National Hurricane Center (Available:https://www.nhc.noaa.gov/news/UpdatedCostliest.pdf), 2018.
[3] "Rebuilding puerto ricos power grid: The inside story," IEEE Spectrum (https://spectrum.ieee.org/energy/policy/rebuilding-puerto-ricos-power-grid-the-inside-story), 2018.
[4] "Facts for features: 2017 hurricane season begins," United States Census Bureau (Available:https://www.census.gov/newsroom/facts-for-features/2017/cb17-ff13-hurricane.html), 2017.
[5] Hurricane Florence: Duke Energy Updates. [Online]. Available: https://www.dukeenergyupdates.com/
[6] Y. Wang, C. Chen, J. Wang, and R. Baldick, "Research on resilience of power systems under natural disastersa review," IEEE Trans. Power Syst, vol. 31, no. 2, pp. 1604–1613, 2016.
[7] D. T. Ton and W. P. Wang, "A more resilient grid: The us department of energy joins with stakeholders in an r&d plan," IEEE Power and Energy Magazine, vol. 13, no. 3, pp. 26–34, 2015.
[8] M. Panteli, P. Mancarella, D. N. Trakas, E. Kyriakides, and N. D. Hatziargyriou, "Metrics and quantification of operational and infrastructure resilience in power systems," IEEE Transactions on Power Systems, vol. 32, no. 6, pp. 4732–4742, Nov 2017.
[9] M. Ouyang, L. Dueñas-Osorio, and X. Min, "A three-stage resilience analysis framework for urban infrastructure systems," Structural safety, vol. 36, pp. 23–31, 2012.
[10] A. Abiri-Jahromi, M. Fotuhi-Firuzabad, M. Parvania, and M. Mosleh, "Optimized sectionalizing switch placement strategy in distribution systems," IEEE Transactions on Power Delivery, vol. 27, no. 1, pp. 362–370, Jan 2012.
[11] J. Kim and Y. Dvorkin, "Enhancing distribution resilience with mobile energy storage: A progressive hedging approach," arXiv preprint arXiv:1803.01184, 2018.
[12] D. N. Trakas and N. D. Hatziargyriou, "Optimal distribution system operation for enhancing resilience against wildfires," IEEE Transactions on Power Systems, vol. 33, no. 2, pp. 2260–2271, 2018.
[13] B. Chen, C. Chen, J. Wang, and K. L. Butler-Purry, "Multi-time step service restoration for advanced distribution systems and microgrids," IEEE Transactions on Smart Grid, pp. 1–1, 2017.
[14] A. Khodaei, "Resiliency-oriented microgrid optimal scheduling," IEEE Transactions on Smart Grid, vol. 5, no. 4, pp. 1584–1591, 2014.
[15] "Enhancing distribution resiliency – opportunities for applying innovative technologies," Electric Power Research Institute, 2013.
[16] Continental United States Hurricane Impacts/Landfalls, 2018. [Online]. Available: http://www.aoml.noaa.gov/hrd/hurdat/All_U.S._Hurricanes.html
[17] "Hazus 4.2," FEMA (Available:https://www.fema.gov/hazus), 2018.
[18] G. J. Holland, "An analytic model of the wind and pressure profiles in hurricanes," Monthly weather review, vol. 108, no. 8, pp. 1212–1218, 1980.
[19] S. R. Han, Estimating hurricane outage and damage risk in power distribution systems. Texas A&M University, 2008.
[20] P. Georgiou, A. G. Davenport, and B. Vickery, "Design wind speeds in regions dominated by tropical cyclones," Journal of Wind Engineering and Industrial Aerodynamics, vol. 13, no. 1-3, pp. 139–152, 1983.
[21] P. J. Vickery and L. A. Twisdale, "Prediction of hurricane wind speeds in the united states," Journal of Structural Engineering, vol. 121, no. 11, pp. 1691–1699, 1995.
[22] R. H. Simpson and H. Saffir, "The hurricane disaster potential scale," Weatherwise, vol. 27, no. 8, p. 169, 1974.
[23] R. Brown, "Cost-benefit analysis of the deployment of utility infrastructure upgrades and storm hardening programs," Quanta Technology, Raleigh, 2009.
[24] J. Kaplan and M. DeMaria, "A simple empirical model for predicting the decay of tropical cyclone winds after landfall," Journal of applied meteorology, vol. 34, no. 11, pp. 2499–2512, 1995.